IgA production requires B cell interaction with subepithelial dendritic cells in Peyer's patches

Andrea Reboldi[1,‡*], Tal I. Arnon[1,†], Lauren B. Rodda[1], Amha Atakilit[2], Dean Sheppard[2] and Jason G. Cyster[1*]

[1]Howard Hughes Medical Institute and Department of Microbiology and Immunology, University of California San Francisco, 513 Parnassus Ave., San Francisco, CA 94143; [2]Lung Biology Center, Department of Medicine, University of California San Francisco, 1550 4th Street, San Francisco, CA 94158, USA.

[‡]Current address: Department of Pathology, University of Massachusetts Medical School, 368 Plantation St., Worcester, MA. 01655, USA.

[†]Current address: Kennedy Institute of Rheumatology, University of Oxford, Roosevelt Drive, Headington, Oxford OX3 7FY, UK.

[*]Address correspondence to andrea.reboldi@umassmed.edu or Jason.Cyster@ucsf.edu

Abstract

Immunoglobulin A (IgA) induction primarily occurs in intestinal Peyer's patches (PPs). However, the cellular interactions necessary for IgA class switching are poorly defined. Here we show that in mice, activated B cells use the chemokine receptor CCR6 to access the sup-epithelial dome (SED) of PPs. There, B cells undergo prolonged interactions with SED dendritic cells (DCs). PP IgA class switching requires innate lymphoid cells, which promote lymphotoxin-β receptor (LTβR)-dependent maintenance of DCs. PP DCs augment IgA production by integrin αvβ8-mediated activation of TGFβ. In mice where B cells cannot access the SED, IgA responses against oral antigen and gut commensals are impaired. These studies establish the PP SED as a niche supporting DC-B cell interactions needed for TGFβ activation and induction of mucosal IgA responses.

IgA, the most abundantly produced antibody isotype in the body, has the dual roles of maintaining homeostasis with the microbiome and protecting from intestinal infection (*1, 2*). Plasma cells located in the lamina propria secrete IgA, but the early stages of IgA production take place mainly in Peyer's patches (PPs)(*3*). PPs are lymphoid organs that are organized into B cell-rich follicles, T cell-rich interfollicular zones and a subepithelial dome (SED) rich in $CD11c^+$ dendritic cells (DCs) that separates the epithelium from the follicles (*4*) (Fig .1A). Gut-derived antigens delivered across specialized epithelial cells continually stimulate PPs and PP follicles harbor chronic T cell-dependent germinal centers (GCs) (*1*). PP GCs contain a high frequency of IgA^+ cells and these give rise to IgA plasma cells. While a number of factors have been implicated in PP B cell switching to IgA, the strongest requirement established *in vivo* is for transforming growth factor β receptor (TGFβR) signaling (*5-7*). However, the cellular interactions involved in promoting TGFβR signaling in PP B cells have been unclear.

B cell intrinsic CCR6 requirement for IgA switching in PPs

Previous studies have shown that CC-chemokine receptor-6 (CCR6)-deficient mice have altered PP organization and reduced antigen-specific IgA levels (*8, 9*). The CCR6 ligand, CCL20, is made abundantly by PP follicle-associated epithelium and DC distribution in the SED was affected by CCR6-deficiency (*8, 9*), though this was not seen in another study (*10*) leaving the mechanism by which CCR6 augments IgA production unclear. An analysis of B cell distribution in wild-type PPs showed that

in addition to their dense presence in follicles, IgD$^+$ B cells were detectable more sparsely within the SED, overlapping with the network of CD11c$^+$ Zbtb46$^+$ DCs in this region (Fig. 1A)(*11*). Although CCR6 is widely expressed by B cells (*12*), the dynamics of PP B cell CCR6 expression have not been determined. A fraction of PP IgD$^+$ and IgD$^-$ B cells had high CCR6 surface staining (Fig. 1B) and further phenotypic analysis based on Fas (CD95), CD11c and IgM expression showed that these B cells were enriched in pre-GC and memory B cells, respectively (Suppl. Fig. S1A). To confirm that PP IgD$^+$CCR6$^+$Fas$^+$CD11c$^+$ cells correspond to pre-GC cells (*13, 14*), wild-type follicular B cells were transferred to monoclonal MD4 Ig-transgenic mice that have little endogenous PP GC activity. A large fraction of the transferred polyclonal B cells, likely stimulated by intestinal antigen in PPs, acquired an IgD$^-$ CCR6$^-$CD38$^-$GL7$^+$ GC phenotype after one week (Fig. 1C). Tracking cell differentiation and division at 3 and 4 days after transfer established that CCR6 was upregulated prior to the appearance of IgD$^-$ GC B cells (Fig. 1D). Fas and CD11c were upregulated with a similar time course (Suppl. Fig. S1B). Some cells that had undergone 4 or more divisions were CCR6^{hi}IgD$^{lo/-}$ (Fig. 1D and Suppl. Fig. S1B), indicating that the CCR6$^+$IgD$^-$ gate (Fig. 1B and Suppl. Fig. S1B) may contain some pre-GC cells as well as memory B cells.

In accord with this CCR6 expression pattern, pre-GC and memory B cells, but not follicular or GC B cells, efficiently migrated towards CCL20 in a CCR6 dependent manner (Fig. 1E and Suppl. Fig. S1C). By contrast, PP DCs showed little migration to CCL20 while responding well to CCL21 and CXCL12 (Suppl. Fig. S1D). CCR6 levels

and function were upregulated in follicular B cells shortly after B-cell receptor (BCR) engagement *in vitro* with anti-IgM (Suppl. Fig. S1E), though not after incubation with anti-CD40, consistent with *in vitro* findings for CCR6 function in activated human B cells (*15*). However, tracking polyclonal B cell activation in PPs using the adoptive transfer system revealed that B cells required CD40 and CD40L for CCR6 upregulation *in vivo* (Fig. 1F and Suppl. Fig. S1F). Together these data provide evidence that CCR6 induction in naïve B cells responding to endogenous PP-associated antigens involves CD40-dependent interactions with helper T cells. Pre-GC cells also had slightly higher amounts of CXCR4, CXCR5 and CCR7 than naïve B cells though their response to the corresponding chemokines was not increased compared to naïve B cells (Fig. 1E and Suppl. Fig. S1G).

To determine whether CCR6 upregulation could be sufficient to control B cell localization to the SED within PPs, B cells from bone marrow (BM) chimeras transduced with CCR6-encoding retrovirus were transferred to wild-type recipients. Three days later the CCR6-overexpressing B cells, identified by expression of a Thy1.1 reporter, were situated preferentially in the SED (Fig. 1G and Suppl. Fig. S2A). In contrast, B cells transduced with the control retrovirus were distributed uniformly within the follicle and SED (Fig. 1G and Fig. S2A). To test whether CCR6 was necessary for B cell localization in the SED, we examined B cell distribution in 50:50 mixed BM chimeras that contained CCR6-deficient or littermate control (Igh^b) cells mixed with wild-type (Igh^a) cells. Notably, CCR6-deficient and wild–type B cells were equally represented in the follicle, but CCR6-deficient B cells were unable to

migrate into the SED (Fig. 1H and Suppl. Fig. S2B). Using the procedure of adoptive cell transfer into MD4 hosts we found that B cells accessed the SED in a CCR6-dependent manner within 4 days of activation by endogenous antigen (Fig. 1I and Suppl. Fig. S2C).

Since CCR6 upregulation on follicular B cells is associated with the transitional stage between naive and GC B cell phenotypes, we sought to directly test the significance of CCR6 in PP B cell fate. We used mixed wild-type (Igh^a): CCR6-deficient (Igh^b) BM chimeras to determine the intrinsic role of CCR6 in B cells and ensure that other CCR6-dependent properties of PPs were intact (*8-10, 16*). CCR6-deficient GC B cells in these chimeras suffered reduced switching to IgA compared to wild-type GC B cells in the same animals, and showed instead an increased propensity for switching to IgG1 (Fig. 2A). In accord with most PP IgA^+ cells being GC B cells (Fig. 2B), the frequency of IgA^+ cells was decreased amongst total *Ccr6*$^{-/-}$ B cells (Fig. 2C and Suppl. Fig. S3A). Analysis of mesenteric LNs (MLNs) in the same animals showed only a low frequency of IgA^+ cells and no impact of CCR6-deficiency (Suppl. Fig. S3B). CCR6-deficiency did not significantly affect the fraction of PP B cells with pre-GC, GC or memory phenotypes (Suppl. Fig. S3C). Analysis of wild-type and CCR6-deficient cells cotransferred to MD4 hosts showed that the early appearance of IgA^+ GC cells was CCR6-dependent (Fig. 2D) and again CCR6-deficiency did not affect the induction of pre-GC, GC or memory cells (Suppl. Fig. S3D). IgA class switching *in vitro* was not affected by CCL20 (Suppl. Fig. S3G), consistent with the CCR6 requirement being to support B cell positioning within the PP. Interestingly, the

mixed chimeras also had reduced frequencies of *Ccr6*$^{-/-}$ Th17 cells in PPs (Suppl. Fig. S3F). However, since the defective IgA response was specific to the allotype marked CCR6-deficient B cells, actions of the receptor in other cell types are unable to account for the CCR6 requirement in B cells. The inability to undergo productive IgA class switch in PPs had a significant impact on mucosal IgA. In mixed chimeras, free IgA derived from CCR6-deficient B cells was underrepresented in fecal pellets (Fig. 2E), and CCR6-deficient B cells made a diminished contribution to the IgA coating intestinal bacteria (Fig. 2F). The role of CCR6 in controlling B cell class switching to IgA was not restricted to the homeostatic situation since following oral immunization of mixed BM chimeras with cholera toxin (CT), a potent lethal toxin that causes severe diarrhea, the IgA response was dominated by antibody derived from the wild-type B cells (Fig. 2G).

The IgA response against intestinal commensals is thought to involve both T-independent and T-dependent antibody production (*17, 18*). Since the great majority of IgA^{+} B cells in wild-type PPs are GC phenotype cells, we anticipated that the role of CCR6 in promoting IgA maybe most prominent during T-dependent responses. To test this we transferred mixtures of wild-type Igh^{a} and *Ccr6*$^{+/+}$ or *Ccr6*$^{-/-}$ Igh^{b} B cells to mice lacking endogenous B cells and that were either T cell-deficient (*Rag1*$^{-/-}$) or T cell-replete (μMT). Allotype-specific analysis of fecal IgA one month later revealed that CCR6 was not required for B cells to mount a T-independent IgA response in the *Rag1*$^{-/-}$ hosts (Fig. 2H), whereas the response in the T cell replete μMT hosts showed a similar CCR6-dependence to the responses in

mixed BM chimeras (Fig. 2H). In accord with the CCR6-dependent secretory IgA responses occurring in PPs, when mixed BM chimeras were generated using lymphotoxin-β-receptor (LTβR)-deficient hosts that are unable to form PPs (*19*), B cell CCR6 expression did not influence total or commensal-bound fecal IgA (Suppl. Fig. S3G).

IgA class switching is initiated in the subepithelial dome

To determine whether IgA class switch recombination (CSR) was initiating at the pre-GC stage, IgA germline transcript (αGT) expression was examined by semi-quantitative and quantitative PCR in naïve (IgD^+CCR6^-), pre-GC (IgD^+CCR6^+), GC (IgD^-CCR6^-) and memory (IgD^-CCR6^+) B cells from wild-type PPs. Pre-GC cells showed a significant increase in αGTs compared to naïve and GC B cells (Fig. 3A). IgA GTs were also abundant in IgD^-CCR6^+ B cells, perhaps reflecting the presence of both late stage pre-GC cells and memory-cell derived pre-GC cells in this gate. Although IgA is the major memory B cell isotype, a fraction of the cells in this gate are unswitched (Suppl. Figs. S3H and S1A). We also detected mature, rearranged, Iμ-Cα transcripts and switch circle transcripts (Iα-Cμ) in the pre-GC cells, though in this case the levels were higher in IgD^-CCR6^- GC B cells as expected from the high fraction of IgA^+ B cells in the GC (Fig. 3B). Consistent with switching initiating in the pre-GC compartment, AID transcripts were elevated in pre-GC compared to naïve B cells (Fig. 3B) and the frequency of AID-GFP^+ cells was higher (Fig. 3C). Although

AID expression was lower in pre-GC than in GC cells (Fig. 3B), the amounts of AID required for CSR are less than required for somatic hypermutation of V regions (*20*).

Lymphotoxin-dependent PP dendritic cells are required for IgA switching

Based on the above kinetic and anatomical findings we reasoned that PP B cells might travel to the SED to receive a stimulus that dictated IgA class switch. The SED is a CD11c$^+$ Zbtb46$^+$ DC rich area (Fig. 1A), containing mainly CD11b$^+$ and CD11b-CD8-double negative (DN) DCs, with CD8$^+$ DCs localized in the interfollicular region (IFR) (*4, 9, 21, 22*). CD11c$^+$ DCs were minimally detected in PP GCs (Suppl. Fig. S4A). *In vitro* studies with human and mouse cells have shown B cell-DC co-culturing can augment IgA switching, though a role for such interactions *in vivo* has not been established (*23-29*). To test whether SED DCs were important for B cell IgA switching, we sought to identify perturbations affecting these DCs. LTβR signaling contributes to CD11b$^+$ DC homeostasis in the spleen (*30*), but whether it has a role in maintaining DCs in PPs is unknown. Analysis of *Ltbr* transcripts in sorted DC subsets from PPs showed that CD11b$^+$ and DN DCs had high expression (Fig. 4A) and these cells were positive for surface LTβR by flow cytometry (Fig. 4A and Suppl. Fig. S4B). When wild-type mice were reconstituted with *Ltbr*$^{-/-}$ BM, they had a deficiency in CD11b$^+$ and DN DCs, whereas CD8$^+$ DCs were less affected (Fig. 4B). Importantly, in these same chimeras, B cell switching to IgA was reduced and switching to IgG1 was increased (Fig. 4C). A similar defect in the balance between IgA and IgG1 class switch was observed in *Ltbr*$^{-/-}$: Itgax-diphtheria toxin receptor

(CD11c-DTR) mixed BM chimeras that had been treated with diphtheria toxin (DT) such that most DCs remaining in the animals were LTβR-deficient whereas all hematopoietic $CD11c^-$ cell types were 50% wild-type (Fig. 4D). In a reciprocal experiment, we tested whether increased LTα1β2-LTβR signaling was sufficient to promote SED DC accumulation and IgA class switch by examining PPs from transgenic mice overproducing LTα1β2 (*30*). In these animals, $CD11b^+$ DCs were increased in number and a greater fraction of GC B cells had switched to IgA compared to littermate controls (Fig. 4E, F). The transcription factor BATF3 controls the development of $CD8a^+$ DCs (*31*) and mice reconstituted with *Batf3*$^{-/-}$ BM showed a near absence of $CD8a^+$ DCs in PPs. (Suppl. Fig S4C). In these mice B cell switching to IgA was normal (Suppl. Fig S4D), indicating that $CD8a^+$ DCs are dispensable for PP IgA class switching.

A concern with the above studies was that chronic LTβR-deficiency in DCs might lead to distant alterations such as changes in the microbiome that have indirect effects on IgA class switching. To address this concern, we used the adoptive transfer approach introduced above (Fig. 1C). Treatment with LTβR-Fc, an LTα1β2 antagonist, during the short period of the transfer decreased the number of $CD11b^+$ DCs (Fig. 4G) and reduced the ability of the transferred B cells to undergo IgA class switch (Fig. 4H), without impacting their participation in the GC reaction (Fig. 4H Taken together, these findings provide strong evidence that LTβR signaling in DCs is directly required for promoting B cell IgA class switching.

Innate lymphoid cells maintain PP dendritic cells required for IgA switching

Innate lymphoid cells type-3 (ILC3, also known as lymphoid tissue inducer cells) are an important source of LTα1β2 for LN and PP organogenesis and during mucosal immune responses (*1, 29, 32, 33*). ILC3s in PPs expressed high levels of surface LTα1β2 (Fig. 5A). Although a previous study showed ILC3-derived LT augmented lamina propria IgA responses, the mice analyzed in that study were PP-deficient, preventing any assessment of the ILC3 role in PP IgA responses (*29*). In order to test the importance of ILC3s in controlling IgA class switch in PPs, we reconstituted irradiated mice using BM cells deficient for RORγt, a transcription factor essential for ILC3 development (*34*). B cells in chimeras lacking ILC3s showed an impaired ability to undergo IgA class switch and an increased propensity to switch to IgG1 compared to B cells from wild-type chimeras (Fig. 5B). These finding suggested that RORγt$^+$ cells were critical in promoting IgA class switch. However, RORγt (encoded by *Rorc*) is expressed not only in ILC3s, but in various T cell types (*35*). To further define the ILC contribution to B cell class switch, we reconstituted irradiated mice with wild-type BM, *Rorc*$^{-/-}$ BM or a mixture of *Rorc*$^{-/-}$ and Rag1$^{-/-}$ BM. In the latter mice the BM mixture could give rise to ILC3s (from the *Rag1*$^{-/-}$ BM) but none of the RORγt-dependent T cell populations. Importantly, while animals lacking RORγt in all hematopoietic cell types showed decreased IgA and increased IgG1 class switch, the animals reconstituted with a mix of *Rorc*$^{-/-}$ and *Rag1*$^{-/-}$ BM showed IgA and IgG1 class switching similar to animals reconstituted with wild-type BM (Fig. 5C). Consistent with ILC3s promoting IgA switching via effects on DCs, the number of

CD11b$^+$ and DN DCs was reduced in the chimeras lacking ILC3s (*Rorc*$^{-/-}$ chimeras) but not in those selectively lacking RORγt-dependent T cells (*Rorc*$^{-/-}$: *Rag1*$^{-/-}$ chimeras, Suppl. Fig. S5A). These results provide strong evidence that ILC3s are the only RORγt-dependent population critical in controlling B cell class switch to IgA in PPs.

To evaluate the role of lymphotoxin on ILC3s in controlling B cell class switch, we made *Rorc*$^{-/-}$: *Lta*$^{-/-}$ mixed BM chimeras. In such animals all the RORγt$^+$ cells are LTα deficient, whereas 50% of the RORγt$^-$ cells are wild–type for LTα. When ILC3s lacked LTα, GC B cells class switched preferentially to IgG1 over IgA (Fig. 5D). These mice also showed a deficiency in CD11b$^+$ and DN DCs, in accord with the dependence of these DCs on LTβR (Suppl. Fig. S5A). The ILC3-deficient mice also had a reduction in CD8$^+$ DCs suggesting additional influences of these cells on DC maturation. Although B cells are an established source of LTα1β2 within follicles (*19*), they express considerably less of this cytokine than ILC3s (Suppl. Fig. S5B) and in chimeric animals selectively lacking LTα1β2 from B cells, PP GC IgA$^+$ cell frequencies and CD11b$^+$ DC frequencies were normal (Suppl. Fig. S5C). Finally, using RORgt-eGFP reporter mice to track RORγt$^+$ cell distribution in PPs, RORgt$^+$CD3$^-$ ILC3s were found in the SED making contact with CD11c$^+$ DCs (Fig. 5E and Suppl. Fig. S5D). These results indicate that in PPs B cell class switching is controlled by the LT-LTβR axis, likely through direct interaction between ILC3s expressing LTα1β2 and SED DCs expressing LTβR.

B cells undergo prolonged interactions with PP subepithelial dome DCs

To determine whether B cells in the SED were interacting with DCs we performed intravital imaging using two-photon laser-scanning microscopy (TPLSM). CD11c-YFP mice were injected with CFP^+ B cells and 10-14 days later individual PPs were surgically exposed and stabilized for imaging by attachment to a platform placed over the mouse abdomen (*36*). Subepithelial dome B cells were identified as being situated in the YFP^+ cell-rich area just beneath the epithelial layer. Contours were drawn immediately internal to the YFP^+ cells in each z-plane and used to generate a three-dimensional surface to separate the SED and follicle (Fig. 6A and Suppl. Movie 1). B cells within the SED or follicle moved with similar velocities (Fig. 6B), but B cells within the SED showed smaller displacement indicating a greater amount of confinement (Fig. 6C). On average, two-thirds of B cells in the SED engaged in short (Scan) or long (Pause) interactions with DCs during 30 minute imaging sessions (Fig. 6D and 6E and Suppl. Movies 2 and 3). To examine B cell migration between follicle and SED, the tracks of cells that crossed between zones were manually annotated. As well as observing B cells migrating from the follicle into the SED, we observed B cells moving in the reverse direction, from the SED into the follicle in some cases following long, seemingly directed tracks (Fig. 6F and Suppl. Movie 4). When B cells were incubated *in vitro* with CCL20, CCR6 became downregulated (Suppl. Fig. S5E) and we suggest that ligand-mediated receptor desensitization over time allows follicular chemoattractant cues to dominate over CCL20 and attract cells away from the SED.

DC integrin αvβ8 is required for TGFβ activation and induction of IgA switching

Since our findings indicated that interaction between B cells and DCs in the SED was required in order to achieve a successful IgA class switch, we investigated the factors involved in this interaction. Several molecules have been described as promoting IgA class switch *in vivo* (*26, 28, 37*), however the most profound phenotype has been reported in mice where TGF-βRII was specifically deleted in B cells (*6*). Activated B cells abundantly express TGFβ transcripts ((*38*) and B cell deficiency in this cytokine leads to a reduction in fecal IgA (*7*). TGFβ activation can be mediated by αvβ6 or αvβ8 integrins binding to latency associated peptide (LAP) and exerting forces that liberate the active cytokine (*39*). $CD11b^+$ and DN DCs in PPs showed abundant transcripts for the Itgb8 (β8) and Itgav (αv) integrin chains (Fig. 7A) and a subset of these DCs had surface expression of the integrin (Fig. 7B). We therefore tested whether DC expression of integrin β8 was required for IgA switching. Irradiated hosts reconstituted with BM from *Itgb8$^{flox/flox}$ Cd11c-Cre* mice showed a defect in IgA class switch in PP GCs, and a propensity toward increased IgG1 class switch (Fig. 7C). By contrast, β8-deficiency did not affect the frequency of IgA^+ or $IgG1^+$ B cells in MLNs (Suppl. Fig. S5F). Short-term treatment with anti-β8 *in vivo* reduced the ability of transferred naïve B cells to undergo IgA class switch in PPs (Fig. 7D), making it unlikely that the switching defect was due to indirect effects of DC β8-deficiency. Moreover, when DCs deficient for β8 were sorted from PPs and

co-cultured *in vitro* with stimulated B cells, they failed to support IgA class switch whereas control DCs supported robust IgA switching (Fig. 7E). Blocking TGFβ signaling in these B cell – DC co-cultures using anti-TGFβ, anti-LAP or anti-β8 reduced the ability of B cells to undergo IgA class switch (Fig. 7F). DC subset analysis revealed that CD11b$^+$ DCs were able to induce IgA class switch *in vitro*, in accord with their integrin β8 and LTβR expression (Fig. 7G). Finally, using BM-derived DCs we found that LTβR engagement with an agonistic antibody led to a weak but reproducible induction of β8 integrin expression (Fig. 7H). Retinoic acid (RA) has an established role in augmenting IgA production, possibly through actions on DCs (*40*). RA treatment of the DC cultures led to a slightly greater β8 integrin induction than LTβR agonism and when the two stimuli were combined, they acted in an additive manner (Fig. 7H).

The increased switching *in vivo* to IgG1 under conditions of reduced IgA switching may be a consequence of the ready availability of IL4 in PPs since it is highly expressed by PP Tfh cells (Suppl. Fig. S5G). Consistent with this interpretation, in irradiated hosts reconstituted with BM from IL4R-deficient mice there was an almost complete absence of IgG1$^+$ cells in PPs (Suppl. Fig. S5H). Under normal conditions, TGFβ-mediated IgA switching may dominate, eliminating the intervening Ig constant regions and thereby limiting switching to IgG1.

Discussion

These studies identify a network of cellular and molecular interactions underpinning the induction of IgA responses in PPs (Suppl. Fig. S6). Following activation by foreign or commensal-derived antigen and receipt of CD40-dependent helper signals, PP B cells upregulate CCR6 and are attracted by CCL20 into the SED where they undergo extensive interactions with $CD11b^+$ DCs. This DC population is maintained by LTα1β2 provided locally by ILC3s. $CD11b^+$ DCs express integrin αvβ8 and promote TGFβ activation during interactions with B cells. Following receipt of TGFβ and likely additional SED-derived signals, B cells return to the follicle by directed migration and participate in the GC response.

Our studies indicate that sustained CCR6 upregulation in PP B cells occurs in a CD40 and thus most likely T cell-dependent manner, and CCR6-deficiency strongly affected T-dependent IgA responses. How CD40 signaling promotes sustained CCR6 expression is not yet clear. Since BCR engagement is sufficient to promote CCR6 upregulation *in vitro*, it remains possible that CCR6 augments certain T-independent IgA responses, with expression perhaps being sustained by other inputs such as from Toll like receptor ligands. It is notable that memory B cells in PPs have high amounts of CCR6 and we speculate that they have privileged access to the SED, perhaps facilitating more rapid exposure to newly arriving antigens.

A key source of TGFβ1 for intestinal IgA production is the B cells themselves (*7*). However, B cell TGFβ1-deficiency does not cause a complete block in IgA production. Given the widespread expression of TGFβ family members

(Immgen.org) we consider it likely that more than one cell type contributes latent TGFβ for DC-mediated activation and triggering of IgA switching,. A number of other signals have been implicated in promoting IgA production including RA, iNOS, APRIL and IL6 (*24, 28, 37, 40*) and our studies do not exclude a role for these mediators in directly or indirectly supporting IgA class switching in PPs. In particular, we suggest that RA helps establish an environment where αvβ8^{+} DCs can develop or be maintained. Although β8-integrin deficient mice were not reported to have reduced serum IgA (*41*), these mice suffer from inflammatory disease due to Treg cell deficiency and this likely allows other factors to induce IgA switching or to generate active TGFβ. Consistent with our findings, a recent study of lung DCs noted a correlation between DC *Itgb8* transcript expression and induction of TGFβ-dependent IgA switching (*42*). We speculate that during B cell–DC interactions in PP SEDs, synaptic contacts form where DC αvβ8 exerts force on TGFβ-LAP tethered on the B cell, leading to TGFβ activation (*39*) and engagement of B cell TGFβR to induce isotype switching. By defining a network of interactions required for IgA switching, this study identifies approaches that could be used to augment IgA responses while also defining sites for defects that could underlie IgA deficiency, the most common immune deficiency syndrome in humans (*43*).

Methods

Mice. Wild-type and Ly5.2 (CD45.1) congenic C57BL/6 (B6) mice, 6–12 weeks old, were from National Cancer Institute. *Lta-/-, Ltbr-/-, Igh^{a}, , MD4-Ig tg, and Lt-tg* (line *Ltb*10 (*44*)) mice were from an internal colony. *Itgax (Cd11c)-cre Itgb8fl/fl* mice (*41*) were backcrossed to C57BL/6J for 10 generations. *Itgax-DTR*, *Ccr6-/-*, *Rorc-/-*, *Rag1-/- , Batf3-/-*, *Cd40-/-* and AID-GFP mice were from Jackson laboratories. IL4-hCD2

(KN2) and *Il4ra-/-* mice were kindly provided by the Locksley lab. Animals were housed in a specific pathogen–free environment in the Laboratory Animal Research Center at UCSF and all experiments conformed to the ethical principles and guidelines approved by the UCSF Institutional and Animal Care and Use Committee.

Flow Cytometry. Spleen, PPs and mLN cell suspensions were generated by mashing the organs through 70-µm cell strainers. For DC isolation, PPs and mLN were digested with 1.6mg type II collagenase (Worthington Biochemical) and DNase I for 10min at 37°C. Digested PPs were mashed into single cell suspension through a 70µm cell strainer in PBS buffers containing 2% FCS and 2mM EDTA. Cells were stained with Abs to CD4 (GK1.5), B220 (RA3-6B2), CD19 (1D3),IgD (11-26c.2a), CD95 (Jo2), GL7, CD38 (90), CCR6 (140706), CD8 (53), MHCII (AF6-120.1), IgA (1040-09), IgG1 (RMA1-1), CD11c (N418), CD11b (M1/70), CD45.1 (A20), CD45.1 (104) (from Biolegend, BD Biosciences, rnBiotech or eBioscience). Biotin conjugates were detected with streptavidin Qdot605 (Invitrogen). To detect intracellular IgA, cells were stained with fixable viability dye (eFluor780; eBioscience) to exclude dead cells then stained for surface antigens, treated with BD Cytofix Buffer and Perm/Wash reagent (BD Biosciences), and stained with anti–IgA antibody.

Immunohistochemistry and Immunofluorescence Microscopy.
For immunohistochemistry, cryosections of 7 µm were acetone fixed and stained as described (*45*) with combinations of the following antibodies: anti-IgD (11-26c.2a, BD Biosciences), anti-IgD^a (AMS9.1, BD Biosciences), anti-IgD^b (217-170, BD Biosciences) and anti-IgM^a (DS-1, BD Biosciences). In some case the slides were counterstained with hematoxylin. For immunofluorescence, tissues were fixed in 4% PFA in PBS for 2 hours at 4^{o}C, washed 3 times for 10 min in PBS, then moved to 30% sucrose in PBS overnight. Tissues were flash frozen in TAK tissue-mounting media the following day, and 7µM sections were cut and then dried for 1 hour prior to staining. Sections were rehydrated in PBS with 1% BSA for 10 min and then stained in primary antibody overnight at 4^{o}C and stained for subsequent steps for 2 hours at room temperature all in PBS with 1% BSA, 2% mouse serum and 2% rat serum. Sections were stained with primary antibodies: Rabbit anti-GFP (polyclonal, Life Technologies), goat anti-mouse IgD (goat polyclonal GAM/IGD(FC)/7S, Cedarlane Labs), Alexa647-conjugated anti-CD11c (N418, Biolegend) and PE-conjugated anti-CD3 (17A2, Biolegend). Sections were then stained with the following secondary antibodies: Alexa488-conjugated donkey anti-rabbit (A-21206, Life Technologies) and AMCA-conjugated donkey anti-goat (705-156-147, Jackson Immunoresearch).

Cell transfer, immunization and transwell assays
For MD4 B cell positioning analysis, 1-2x10^7 MD4 WT or MD4 Ccr6$^{-/-}$ B cells were transfer in C57BL/6 recipients for 3 days before immunizing with 5 mg of HEL i.v. and PPs were harvested at different time points. For polyclonal B cell transfer, MD4 WT recipients were adoptively transferred with 1-2x10^7 splenic B cells from congenic C57BL/6 for the indicated time. In some case B cells were stained with CellTrace Violet (Life technology) according to the manufacturer's protocol. For

LTβR-Fc treatment, mice were treated with LTβR-Fc protein (provided by J. Browning) by i.v. injection of 100 μg of protein every 3.5 days for 7 days. For anti-Itgb8 treatment, mice were treated with neutralizing antibody by i.v. injection of 10 mg/kg of antibody every 3.5 days for 7 days. For anti-CD40L treatment, mice were treated with neutralizing antibody by i.v. injection of 1 mg of anti-mouse CD40L (clone MR1) every 3.5 days for 7 days. For cholera toxin immunization, mice were injected 3 times orally with 10 ug of cholera toxin (EMD Bioscience), oral immunizations were performed 7 days apart and mice were analyzed 7 days after the final immunization. Transwell migration assays were done with 5 μm transwells using 10^6 digested PP cells and enumeration of transmigrated cells by flow cytometry as previously (*46*). Chemokines were obtained from PeproTech or R&D Systems.

Sorting. For DC sorting, PPs and mLN were digested and stained as described above and sorted on a FACSAira III with a 70 μm nozzle. In same cases, DC were isolated from PPs of 8-10 week-old mice that had been injected s.c. in the flank with 5×10^6 B16 murine Flt3L-secreting tumor cells 7-10 days earlier. This treatment led to a approximately 10-fold expansion in total PP DC numbers.

Bone marrow chimeras, retroviral transduction, and DT treatment. Ly5.2 congenic B6 mice were lethally irradiated with either 1,100 or 1,300 rad in split doses and reconstituted with 1–3 x 10^6 BM cells from the indicated donors. Mice were analyzed 10–14 weeks later. For retroviral transduction, PlatE cells were transfected with MSCV retroviral constructs encoding full-length mouse Ccr6 with Lipofectamine 2000 (Invitrogen) following the manufacturer's protocol. For transduction of BM-derived cells, BM cells were harvested 4 days after 5-flurouracil (Sigma) injection and cultured in the presence of recombinant IL-3, IL-6, and mouse stem cell factor (SCF) (100ng/ml, Peprotech). BM cells were spin-infected twice with a retroviral construct expressing Ccr6 and an IRES–Thy1.1 cassette as a reporter. One day after the last spin infection the cells were injected into lethally irradiated C57BL/6 recipients. 8-12 weeks later splenic B cells were isolated, injected in C57BL/6 recipients and their positioning in PP was assessed 3 days later. For DT treatments, BM chimeras received 4 ng DT (EMD Bioscience) per gram body weight every 72h for 3 weeks.

Rag1-/- and μMT cells transfer. Splenic B cells were sorted on a FACSAira III with a 70 μm nozzle as CD3, CD43, CD4, CD8, CD11c, Ly6C, Ly6G, CD90 neg and 10^6 cells from each genotype were transferred i.v. Recipients were analyzed 4 weeks later.

ELISA. Ninety-six-well plates (Thermo Fisher Scientific) were coated with purified anti-IgA (RMA-1, BD) or 0.5nM ml GM1 followed by 0.5 ug/ml CT overnight at 4 °C (*47*). The plates were washed and clocked with PBS/5% BSA before diluted fecal samples were added and twofold serial dilution was made. Samples were incubated overnight at 4 °C, followed by biotinylated anti-mouse antibodies: anti-IgA (C10-1, BD), anti-IgA^a and anti-IgA^b (Hy16 and HISM2, UCSF Hybridoma Core) at 1 ug/ml in PBS/0.1% BSA. Detection antibodies were labeled by streptavidin-conjugated

horseradish peroxidase (HRP), and visualized by the addition of Substrate Reagent Pack (R&D). Color development was stopped with 3 M H_2SO_4. Purified mouse IgA (Southern Biotech) served as standard and was purchased from Southern Biotech. Absorbances at 450 nm were measured on a tunable microplate reader (VersaMax, Molecular Devices). Antibody titers were calculated by extrapolating absorbance values from standard curves where known concentrations were plotted against absorbance using SoftMax Pro 5 software.

Flow cytometric analysis of IgA-bound bacteria. Flow cytometric analysis of gut bacteria in feces was as described (*48*). Briefly, fecal pellets were suspended in filtered PBS (100 µl to 10 mg feces), homogenized well and centrifuged at 400 g for 5 min to remove larger particles from the fecal suspension. Supernatant containing bacteria was centrifuged at 8000 g for 10 min. The bacterial pellet was blocked on ice in 1 ml of BSA/PBS (1 % w/v) for 15'. Samples were spun at 8000 g for 10 min. Bacteria were stained with anti-IgA^a and anti-IgA^b on ice for 20 min and washed with PBS. Finally, bacterial pellets were resuspended in SYBR green I (1/10000 (v/v) dilution Life Technologies) and analyzed using an LSRII flow cytometer.

RNA Isolation and Real-Time RT-PCR. Total RNA was isolated from sorted DCs and B cells from PPs with the Trizol reagent (Life technology) following the manufacturer's protocol. Real-time PCR was performed using SYBR Green PCR Mix (Roche) and an ABI prism 7300 sequence detection system (Applied Biosystems, Foster city, CA).
Hprt For:AGGTTGCAAGCTTGCTGGT, Rev:TGAAGTACTCATTATAGTCAAGGGCA
Ltbr For: CCAGATGTGAGATCCAGGGC, Rev: GACCAGCGACAGCAGGATG
Itgb8 For: CTGAAGAAATACCCCGTGGA, Rev: ATGGGGAGGCATACAGTCT
Itgav For: CGCCTATCTTCGGGATGAATC, Rev: CCAACCGATACTCCATGAAAA
aGT For: CCAGGCTAGACAGAGGCAAG, Rev: CGGAAGGGAAGTAATCGTGA
Aicda For: GCCAAGGGACGGCATGAG, Rev: GATGTAGCGTAGGAACAACAA
Semi-quantitative RT-PCR on sorted B cells for AID, alpha germline transcripts (αGT), Iμ-Cα, and Iα-Cμ were amplified with primers and conditions described before (26).

In vitro culture. For CCR6 upregulation, splenic B cells were stimulated with 10 ug/ml anti-IgM (F(ab')2 goat anti-mouse IgM, Jackson Immunoresearch) for the indicated time. For IgA class switch B-DC coculture experiments, MACS-isolated splenic B cells (typically at 50,000 cells per well) were stimulated with 10 ug/ml anti-IgM and 20 ug/ml anti-CD40 (clone FGK4.5, UCSF Hybridoma Core) in the presence or absence of sorted DCs at a ratio of 1:1 for 5 days. The sorted DCs were from PPs of untreated mice in all cases except for the experiment involving sorted DC subsets where they were from B16-Flt3L treated mice. For IgA class switch in the absence of DCs, MACS-isolated splenic B cells were stimulated with 10 ug/ml anti-IgM and 20 ug/ml anti-CD40 (clone FGK4.5, UCSF Hybridoma Core) in the presence of TGFβ (2 ng/ml) and RA (100 nM) for 5 days.

For BMDCs, 5 × 10^6 BM cells were cultured in 10 cm tissue culture dishes in 10 ml of medium supplemented with supernatants from 3T3 cells transfected with the gene-encoding murine GM-CSF 7 days. Cells were treated with 1 μg/ml LTβR agonistic antibody (clone 3C8) and 100 nM RA every 3.5 days for 7 days.

Intravital two-photon laser-scanning microscopy (TPLSM) of PPs. Mice were anaesthetized by intraperitoneal injection of 10 ml kg−1 saline containing xylazine (1 mg ml−1) and ketamine (5 mg ml−1). Maintenance doses of intramuscular injections of 4 ml kg−1 of xylazine (1 mg ml−1) and ketamine (5 mg ml−1) were given approximately every 30 min. An incision was made in the abdominal wall and the small intestine was gently stretched and scanned by eye to identify PP structures. Only small areas (1-2cm long) were exposed at any time. Once a PP was located, the area was embedded in warm saline and stabilized by placing a spring-loaded platform over the mouse and screwed down until the cover glass made contact with the PP. The tissue was placed with the interface between the intestinal lumen and PP facing upwards in an orientation that allowed maximal viewing of the SED. The mouse was placed on a Biotherm stage warmer at 37 °C (Biogenics) for the duration of the imaging. Images were acquired with ZEN2009 (Carl Zeiss) using a 7MP two-photon microscope (Carl Zeiss) equipped with a Chameleon laser (Coherent). For video acquisition, a series of planes of 2 or 3μm z-spacing spanning a depth of 30–69 μm were collected every 15–20 s. Excitation wavelengths were 850–890 nm. Since most of the transferred CFP^+ B cells occupied the follicular compartment, we used automated tracks (generated by Imaris 7.4.2 ×64, Bitplane) to highlight the follicular region, as previously described (*36*). The SED was identified by the presence of CD11c-YFP DCs and by its typical shape and location above the follicles. The inter-follicular regions, which are also rich with CD11c-YFP DCs, were identified based on their distinct positioning and were excluded from analysis. Videos were made and analyzed using Imaris 7.4.2 ×64 (Bitplane). To track cells, surfaces seed points were created and tracked over time. Tracks were manually examined and verified. Data from cells that could be tracked for at least 15 min were used for analysis. Data presented in figure 3 were collected from 4 independent movies, some of the movies were split into 2 x 30 min segments and analyzed using Imaris (Bitplane AG), MATLAB (MathWorks), and MetaMorph software. figure 3D, the contact time between B cells and DCs in the SED were measured manually (n=150 B cells, derived from 4 independent movies). The behavior of a B cell engaged in prolonged interactions was defined as ‘pause’ (5-25min contact time), ‘scan’ (2-5min contact), or ‘no contact’ when spending less than 2 min in association with a DC. Statistical analysis was performed using Prism software (GraphPad Software).

References

1. S. Fagarasan, S. Kawamoto, O. Kanagawa, K. Suzuki, Adaptive immune regulation in the gut: T cell-dependent and T cell-independent IgA synthesis. *Annu. Rev. Immunol.* **28**, 243-273 (2010).
2. E. Slack, M. L. Balmer, A. J. Macpherson, B cells as a critical node in the microbiota-host immune system network. *Immunol. Rev.* **260**, 50-66 (2014).
3. S. W. Craig, J. J. Cebra, Peyer's patches: an enriched source of precursors for IgA-producing immunocytes in the rabbit. *J. Exp. Med.* **134**, 188-200 (1971).
4. A. Iwasaki, B. L. Kelsall, Localization of distinct Peyer's patch dendritic cell subsets and their recruitment by chemokines macrophage inflammatory protein (MIP)-3alpha, MIP-3beta, and secondary lymphoid organ chemokine. *J. Exp. Med.* **191**, 1381-1394. (2000).
5. F. W. van Ginkel *et al.*, Partial IgA-deficiency with increased Th2-type cytokines in TGF-beta 1 knockout mice. *J. Immunol.* **163**, 1951-1957 (1999).
6. B. B. Cazac, J. Roes, TGF-beta receptor controls B cell responsiveness and induction of IgA in vivo. *Immunity* **13**, 443-451 (2000).
7. M. J. Gros, P. Naquet, R. R. Guinamard, Cell intrinsic TGF-beta 1 regulation of B cells. *J. Immunol.* **180**, 8153-8158 (2008).
8. D. N. Cook *et al.*, CCR6 mediates dendritic cell localization, lymphocyte homeostasis, and immune responses in mucosal tissue. *Immunity* **12**, 495-503 (2000).
9. R. Varona *et al.*, CCR6-deficient mice have impaired leukocyte homeostasis and altered contact hypersensitivity and delayed-type hypersensitivity responses. *J. Clin. Invest.* **107**, R37-45 (2001).
10. X. Zhao *et al.*, CCL9 is secreted by the follicle-associated epithelium and recruits dome region Peyer's patch CD11b+ dendritic cells. *J. Immunol.* **171**, 2797-2803 (2003).
11. M. Ebisawa *et al.*, CCR6hiCD11c(int) B cells promote M-cell differentiation in Peyer's patch. *Int. Immunol.* **23**, 261-269 (2011).
12. T. Kucharzik, J. T. Hudson, 3rd, R. L. Waikel, W. D. Martin, I. R. Williams, CCR6 expression distinguishes mouse myeloid and lymphoid dendritic cell subsets: demonstration using a CCR6 EGFP knock-in mouse. *Eur. J. Immunol.* **32**, 104-112 (2002).
13. T. A. Schwickert, B. Alabyev, T. Manser, M. C. Nussenzweig, Germinal center reutilization by newly activated B cells. *J. Exp. Med.* **206**, 2907-2914 (2009).
14. J. J. Taylor, K. A. Pape, M. K. Jenkins, A germinal center-independent pathway generates unswitched memory B cells early in the primary response. *J. Exp. Med.* **209**, 597-606 (2012).
15. F. Liao, A. K. Shirakawa, J. F. Foley, R. L. Rabin, J. M. Farber, Human B cells become highly responsive to macrophage-inflammatory protein-3 alpha/CC chemokine ligand-20 after cellular activation without changes in CCR6 expression or ligand binding. *J. Immunol.* **168**, 4871-4880. (2002).
16. K. G. McDonald *et al.*, CC chemokine receptor 6 expression by B lymphocytes is essential for the development of isolated lymphoid follicles. *Am. J. Pathol.* **170**, 1229-1240 (2007).

17. A. J. Macpherson *et al.*, A primitive T cell-independent mechanism of intestinal mucosal IgA responses to commensal bacteria. *Science* **288**, 2222-2226. (2000).
18. J. J. Bunker *et al.*, Innate and Adaptive Humoral Responses Coat Distinct Commensal Bacteria with Immunoglobulin A. *Immunity* **43**, 541-553 (2015).
19. J. L. Gommerman, J. L. Browning, Lymphotoxin/light, lymphoid microenvironments and autoimmune disease. *Nat. Rev. Immunol.* **3**, 642-655 (2003).
20. L. Yeap *et al.*, Sequence-Intrinsic Mechanisms that Target AID Mutational Outcomes on Antibody Genes. *Cell* **163**, 1124-1137. (2015).
21. B. L. Kelsall, W. Strober, Distinct populations of dendritic cells are present in the subepithelial dome and T cell regions of the murine Peyer's patch. *J. Exp. Med.* **183**, 237-247 (1996).
22. A. Iwasaki, B. L. Kelsall, Unique functions of CD11b+, CD8 alpha+, and double-negative Peyer's patch dendritic cells. *J. Immunol.* **166**, 4884-4890 (2001).
23. J. Fayette *et al.*, Human dendritic cells skew isotype switching of CD40-activated naive B cells towards IgA1 and IgA2. *J. Exp. Med.* **185**, 1909-1918 (1997).
24. M. B. Litinskiy *et al.*, DCs induce CD40-independent immunoglobulin class switching through BLyS and APRIL. *Nat. Immunol.* **3**, 822-829 (2002).
25. A. J. Macpherson, T. Uhr, Induction of protective IgA by intestinal dendritic cells carrying commensal bacteria. *Science* **303**, 1662-1665 (2004).
26. J. R. Mora *et al.*, Generation of gut-homing IgA-secreting B cells by intestinal dendritic cells. *Science* **314**, 1157-1160 (2006).
27. M. Tsuji *et al.*, Requirement for lymphoid tissue-inducer cells in isolated follicle formation and T cell-independent immunoglobulin A generation in the gut. *Immunity* **29**, 261-271 (2008).
28. H. Tezuka *et al.*, Regulation of IgA production by naturally occurring TNF/iNOS-producing dendritic cells. *Nature* **448**, 929-933 (2007).
29. A. A. Kruglov *et al.*, Nonredundant function of soluble LTalpha3 produced by innate lymphoid cells in intestinal homeostasis. *Science* **342**, 1243-1246 (2013).
30. K. Kabashima *et al.*, Intrinsic Lymphotoxin-beta Receptor Requirement for Homeostasis of Lymphoid Tissue Dendritic Cells. *Immunity* **22**, 439-450 (2005).
31. B. T. Edelson *et al.*, CD8alpha(+) dendritic cells are an obligate cellular entry point for productive infection by Listeria monocytogenes. *Immunity* **35**, 236-248 (2011).
32. S. A. van de Pavert, R. E. Mebius, New insights into the development of lymphoid tissues. *Nat. Rev. Immunol.* **10**, 664-674 (2010).
33. S. P. Spencer *et al.*, Adaptation of innate lymphoid cells to a micronutrient deficiency promotes type 2 barrier immunity. *Science* **343**, 432-437 (2014).
34. S. Sawa *et al.*, Lineage relationship analysis of RORgammat+ innate lymphoid cells. *Science* **330**, 665-669 (2010).

35. Ivanov, II *et al.*, The orphan nuclear receptor RORgammat directs the differentiation program of proinflammatory IL-17+ T helper cells. *Cell* **126**, 1121-1133 (2006).
36. T. I. Arnon, R. M. Horton, I. L. Grigorova, J. G. Cyster, Visualization of splenic marginal zone B-cell shuttling and follicular B-cell egress. *Nature* **493**, 684-688 (2013).
37. E. Castigli *et al.*, Impaired IgA class switching in APRIL-deficient mice. *Proc. Natl. Acad. Sci. U. S. A.* **101**, 3903-3908 (2004).
38. V. V. Parekh *et al.*, B cells activated by lipopolysaccharide, but not by anti-Ig and anti-CD40 antibody, induce anergy in CD8+ T cells: role of TGF-beta 1. *J. Immunol.* **170**, 5897-5911 (2003).
39. M. A. Travis, D. Sheppard, TGF-beta activation and function in immunity. *Annu. Rev. Immunol.* **32**, 51-82 (2014).
40. E. J. Villablanca *et al.*, MyD88 and retinoic acid signaling pathways interact to modulate gastrointestinal activities of dendritic cells. *Gastroenterology* **141**, 176-185 (2011).
41. M. A. Travis *et al.*, Loss of integrin alpha(v)beta8 on dendritic cells causes autoimmunity and colitis in mice. *Nature* **449**, 361-365 (2007).
42. D. Ruane *et al.*, Microbiota regulate the ability of lung dendritic cells to induce IgA class-switch recombination and generate protective gastrointestinal immune responses. *J. Exp. Med.* **213**, 53-73 (2016).
43. L. Hammarstrom, I. Vorechovsky, D. Webster, Selective IgA deficiency (SIgAD) and common variable immunodeficiency (CVID). *Clin. Exp. Immunol.* **120**, 225-231 (2000).
44. V. N. Ngo, R. J. Cornall, J. G. Cyster, Splenic T zone development is B cell dependent. *J. Exp. Med.* **194**, 1649-1660. (2001).
45. J. P. Pereira, J. An, Y. Xu, Y. Huang, J. G. Cyster, Cannabinoid receptor 2 mediates the retention of immature B cells in bone marrow sinusoids. *Nat. Immunol.* **10**, 403-411 (2009).
46. V. N. Ngo, H. L. Tang, J. G. Cyster, Epstein-Barr virus-induced molecule 1 ligand chemokine is expressed by dendritic cells in lymphoid tissues and strongly attracts naive T cells and activated B cells. *J. Exp. Med.* **188**, 181-191 (1998).
47. P. Bergqvist *et al.*, Re-utilization of germinal centers in multiple Peyer's patches results in highly synchronized, oligoclonal, and affinity-matured gut IgA responses. *Mucosal Immunol* **6**, 122-135 (2013).
48. S. Kawamoto *et al.*, The inhibitory receptor PD-1 regulates IgA selection and bacterial composition in the gut. *Science* **336**, 485-489 (2012).

Acknowledgements

We thank M. Matloubian for help with the B16-Flt3L, J. Bluestone for the RORγt-GFP, mice, M. Krummel for Zbtb46-GFP mice, M. Rosenblum for the *Baft3*$^{-/-}$ mice, R.Locksley for KN2 mice and *Il4ra*$^{-/-}$ mice, F. Kroese for HISM2 hybridoma, M. Miller for advice regarding intravital microscopy, Y. Xu and J. An for expert technical assistance and O. Bannard for comments on the manuscript. The data presented in

this manuscript are tabulated in the main paper and in the supplementary materials. UCSF has filed a patent (US patent application 14/778,997) describing the αvβ8 blocking antibody used in this manuscript. D.S. and A.A. are listed as inventors. A.R. was a recipient of Irvington postdoctoral fellowship from the Cancer Research Institute. J.G.C. is an Investigator of the Howard Hughes Medical Institute. The work was supported in part by NIAID U19 grant AI077439 (to DS) and RO1 grants AI045073 and AI074847 (to J.G.C).

FIGURE LEGENDS

Figure 1. B cell access to the PP subepithelial dome (SED) is CCR6-dependent.

(A) Representative images of Peyer's patch (PP) dome stained with anti-CD11c (blue) and anti-IgD (brown) (left panel) or with anti-GFP (green) and anti-IgD (blue) (right panel). Dashed white line demarcates the follicle-SED boundary. Scale bar is 20μm. **(B)** Representative flow cytometric analysis of $CD19^+$ B cells in PPs for IgD and CCR6 expression. **(C, D)** Representative FACS staining of transferred CellTrace Violet-labeled polyclonal B cells (red) in MD4 hosts (endogenous B cells, black) for IgD and GL7 at day 7 (C) and IgD and CCR6 at days 3 and 4 after transfer. **(E)** Migration of PP follicular and pre-GC B cells from $Ccr6^{+/+}$ and $Ccr6^{-/-}$ mice to the indicated chemokines. **(F)** Representative CCR6 expression on transferred wild-type (WT) and $Cd40^{-/-}$B cells in MD4 hosts (upper panels) or wild-type B cells in MD4 hosts treated with either isotype control or anti-CD40L antibody (lower panels) after 7 days. **(G)** Representative images of distribution of transferred B cells (Thy1.1, brown) in sections of PP from mice receiving control vector or CCR6-transduced B cells. Slides were counterstained with hematoxylin. **(H)** Representative images of distribution of B cells in PPs of chimaeras reconstituted with 50% Igh^b *Ccr6*$^{+/+}$ or *Ccr6*$^{-/-}$ and 50% Igh^a wild-type BM. Sections were stained to detect *Ccr6*$^{+/+}$ or *Ccr6*$^{-/-}$ B cells (IgD^b, blue) and control B cells (IgD^a, brown). **(I)** Distribution of polyclonal *Ccr6*$^{+/+}$ and *Ccr6*$^{-/-}$ B cells in PPs of mixed transfer MD4 recipients (75% CD45.2 *Ccr6*$^{+/+}$ or *Ccr6*$^{-/-}$ and 25% CFSE CD45.1 wild-type) 4 days after transfer. Sections were stained to detect *Ccr6*$^{+/+}$ or *Ccr6*$^{-/-}$ B cells (CD45.2,

blue) and control B cells (CFSE, brown). Each symbol in (E) represents an individual mouse, and data are pooled from at least three independent experiments. Data in (A), (B), (C), (D), (F), (G), (H) and (I) are representative of at least three independent experiments. *, $p<0.05$; **, $p<0.01$, ***, $p<0.005$ (unpaired Student's T-test).

Figure 2. B cell isotype switching to IgA is CCR6-dependent.

(A) Frequency of WT and *Ccr6*$^{+/+}$ or *Ccr6*$^{-/-}$ GC B cells expressing IgA or IgG1 in PPs from mixed BM chimeras, as determined by FACS. **(B)** GC and memory contribution to IgA^{+} B cell pool in PPs. **(C)** Representative FACS of frequency of WT and *Ccr6*$^{+/+}$ or *Ccr6*$^{-/-}$ B cells expressing IgA or IgG1 in PPs from mixed BM chimeras. **(D)** Representative FACS staining (left panel) and frequency (right panel) of IgA^{+} B cells amongst transferred B cells in MD4 recipient PPs after 7 days. **(E)** Fecal IgA from WT (Igh^{a}) and *Ccr6*$^{+/+}$ or *Ccr6*$^{-/-}$ (Igh^{b}) mixed BM chimeras as measured by allotypic ELISA. **(F)** Percentage of fecal bacteria coated with IgA^{a} or IgA^{b} measured by FACS from mixed BM chimeras as in A. **(G)** Fecal CT-specific IgA from WT (Igh^{a}) and *Ccr6*$^{+/+}$ or *Ccr6*$^{-/-}$ (Igh^{b}) mixed BM chimeras orally treated with CT, measured by allotypic ELISA. **(H)** Fecal IgA from WT (Igh^{a}) and *Ccr6*$^{+/+}$ or *Ccr6*$^{-/-}$ (Igh^{b}) B cells co-transferred in to either *Rag1*$^{-/-}$ or μMT, or from mixed BM chimeras as in A, measured by allotypic ELISA. Each symbol in (A), (B), (E), (F), (G) and (H) represents an individual mouse, and data are pooled from at least three

independent experiments. Data in (C) and (D) are representative of at least three independent experiments. *, $p<0.05$; **, $p<0.01$, ***, $p<0.005$ (unpaired Student's T-test).

Figure 3. Pre-GC B cells in PPs initiate IgA class switch.

(A, B) Representative semi-quantitative **(A)** or quantitative **(B)** RT-PCR on B cells from PPs sorted according to IgD and CCR6 expression, for the indicated transcripts. **(C)** Representative FACS staining (left panel) and frequency (right panel) of AID-GFP$^+$ PP B cells from reporter mice, according to IgD and CCR6 expression. Each symbol in (B) and (C) represents an individual mouse and data are pooled from three independent experiments. Data in (A) are representative of three independent experiments.

Figure 4. LTβR-dependent PP DC support IgA class switching.

(A) Quantitative PCR analysis of Ltbr transcript abundance in the indicated DC subsets from PPs (left panel) and median fluorescence intensity (MFI) ratio for LTβR on the DC subsets from PPs of BM chimeras reconstituted with WT or *Ltbr*$^{-/-}$ BM (right panel). **(B)** Representative FACS staining (left panel) and absolute cell number (right panel) of the indicated DC subset from PPs of BM chimeras reconstituted with WT or *Ltbr*$^{-/-}$ BM, **(C)** Frequency of IgA$^+$ and IgG1$^+$ GC B cells in

PPs from BM chimeras as in B, determined by FACS. **(D)** Frequency of IgA^+ and $IgG1^+$ GC B cells in PP from mixed chimeras reconstituted with CD11c-DTR and either *Ltbr*$^{+/+}$ or *Ltbr*$^{-/-}$ BM, treated with DT for 3 weeks. **(E)** Absolute number of the indicated DC subset from PPs of WT or LT-transgenic (tg) mice. **(F)** Frequency of IgA^+ and $IgG1^+$ GC B cells in PPs from WT or LT-tg mice, as determined by FACS. **(G)** Absolute number of the indicated DC subset from PPs of mice treated with LTβR-Fc or hIgG-Fc for 7 days. **(H)** Representative FACS staining of polyclonal B cells in PPs 7 days after transfer to MD4 recipients that were treated with LTβR-Fc or hIgG-Fc (left panel) and frequency of IgA^+ B cells and GC B cells in PPs amongst transferred B cells (right panels). Each symbol in (A), (B), (C), (D), (E), (F), (G) and (H) represents an individual mouse, and data are pooled from at least three independent experiments. In (B), (C), (D), (E), (F), (G) and (H) *, $p<0.05$; **, $p<0.01$, ***, $p<0.005$ (unpaired Student's T-test); in A, ***, $p<0.005$ (one-way ANOVA with Bonferroni's post-hoc test).

Figure 5. LT- and ILC3-dependence of PP IgA response.

(A) Representative FACS staining showing gating strategy and LTα1β2 on ILC3s in PP of WT mouse using LTβR-Fc. **(B)** Frequency of IgA^+ and $IgG1^+$ GC B cells in PPs from chimeras reconstituted with WT or *Rorc*$^{-/-}$ BM. **(C)** Frequency of IgA^+ and $IgG1^+$ GC B cells in PPs as determined by FACS in BM chimeras reconstituted with WT, *Rorc*$^{-/-}$ or a mix of *Rorc*$^{-/-}$ and *Rag1*$^{-/-}$ BM. **(D)** Frequency of IgA^+ and $IgG1^+$ GC B cells in PPs as determined by FACS in BM chimeras reconstituted with a mix of *Lta*$^{-/-}$

BM and either WT or *Rorc*$^{-/-}$ BM. **(E)** Representative immunofluorescence of PP SED from Rorc(γt)-EGFP mouse stained for the indicated markers. Yellow arrowheads indicate ILC3s proximal to DCs. Scale bar is 20μm. Each symbol in (B), (C) and (D), represents an individual mouse, and data are pooled from at least three independent experiments. Data in (A) and (E) are representative of at least three independent experiments. In B and D,***, $p<0.005$ (unpaired Student's T-test); in C, , ***, $p<0.005$ (one-way ANOVA with Bonferroni's post-hoc test).

Figure 6. PP B cell migration dynamics and interaction with SED DCs.

(A) Representative TPLSM of PP for transferred CFP$^+$ B cells (green) in CD11c-YFP mice. YFP$^+$ cells (red) are shown using volume rendering. White dotted line indicates location of the SED. **(B)** Median velocity and **(C)** displacement versus square root of time of B cells in follicle (black) and in the SED (blue). **(D)** Percentage of B cells in the SED pausing (Pause), scanning (Scan) or not contacting (No contact) CD11c-YFP$^+$ cells. **(E)** Representative time-lapse images of CFP$^+$ B cell interaction with CD11c-YFP$^+$ cell in the SED. Arrowhead highlights a single B cell-DC interaction. (Yellow color is due to bleed-through between channels). Time is shown in min:sec. **(F)** Representative z-projection view of PP follicle and SED of the type in A, showing only the CFP$^+$ B cells. White dotted line, SED–follicle border; yellow lines, tracks of B cells in the follicle; blue lines, track of B cells in the SED; pink lines, tracks of B cells moving from the SED to the follicle; white lines, tracks of B cells moving from the follicle to the SED. Each symbol in (B) and (D), represents an individual mouse, and

data are pooled from at least three independent experiments. Data in (A), (C), (E) and (F) are representative of at least three independent experiments.

Figure 7. DC integrin-β8 promotes TGFβ -dependent IgA switching.

(A) Quantitative PCR analysis of Itgb8 (left panel) and Itgav (right panel) transcript abundance in the indicated DC subsets from PPs. **(B)** Median fluorescence intensity (MFI) ratio for β8 on the indicated DC subsets from PPs of either CD11c-Cre$^-$ (WT) or CD11c-Cre$^+$ *Itgb8$^{fl/fl}$* mice. **(C)** Frequency of IgA$^+$ and IgG1$^+$ GC B cells in PPs of either CD11c-Cre$^-$ or CD11c-Cre$^+$ *Itgb8$^{fl/fl}$* mice as determined by FACS. **(D)** Frequency of IgA$^+$ and IgG1$^+$ GC B cells in PPs 7 days after adoptive transfer in MD4 mice and treatment with either isotype control or anti-β8. **(E)** Frequency of IgA$^+$ splenic B cells upon 5 days of culture with DCs sorted from PPs or mLNs of CD11c-Cre$^-$ or CD11c-Cre$^+$ *Itgb8$^{fl/fl}$* mice. **(F)** Frequency of IgA$^+$ splenic B cells upon 5 days of culture with DCs sorted from PPs and incubated with the indicated antibodies. **(G)** Frequency of IgA$^+$ splenic B cells upon 5 days of culture with the indicated DC subset sorted from PPs. **(H)** Median fluorescence intensity (MFI) for β8 on the BMDCs generated from CD11c-Cre$^-$ or CD11c-Cre$^+$ *Itgb8$^{fl/fl}$* BM upon 7 days of culture and incubation with the indicated reagents. Each symbol in (B), (C), (D), (E), (F), (G) and (H) represents an individual mouse, and data are pooled from at least three independent experiments. Data in (A) are pooled from three independent experiments In B, F and G *, $p<0.05$; **, $p<0.01$, ***, $p<0.005$ (one-way ANOVA with

Bonferroni's post-hoc test); in C, D and E **, $p<0.01$, ***, $p<0.005$ (unpaired Student's T-test).

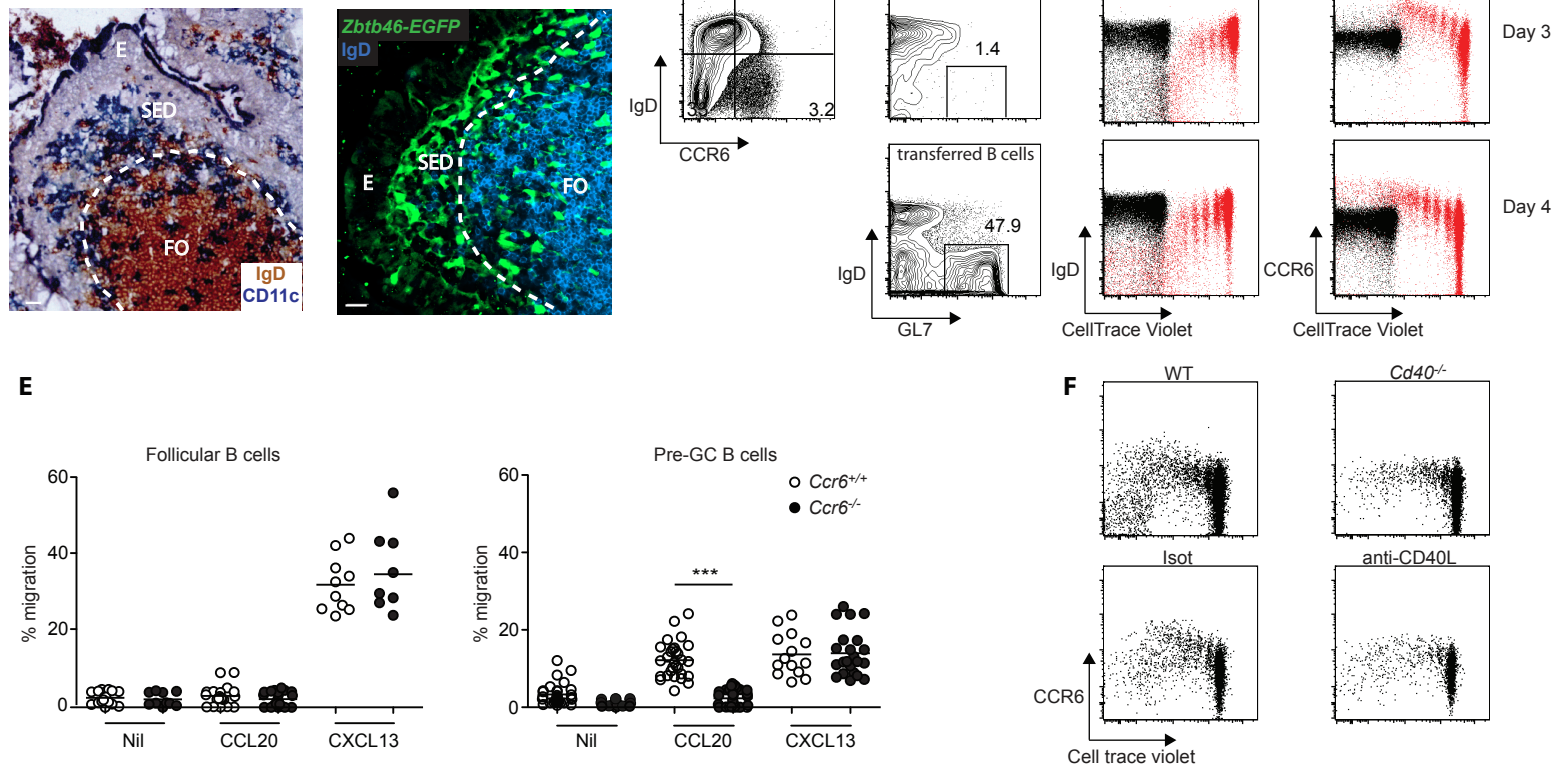

Reboldi at al.
Figure 1

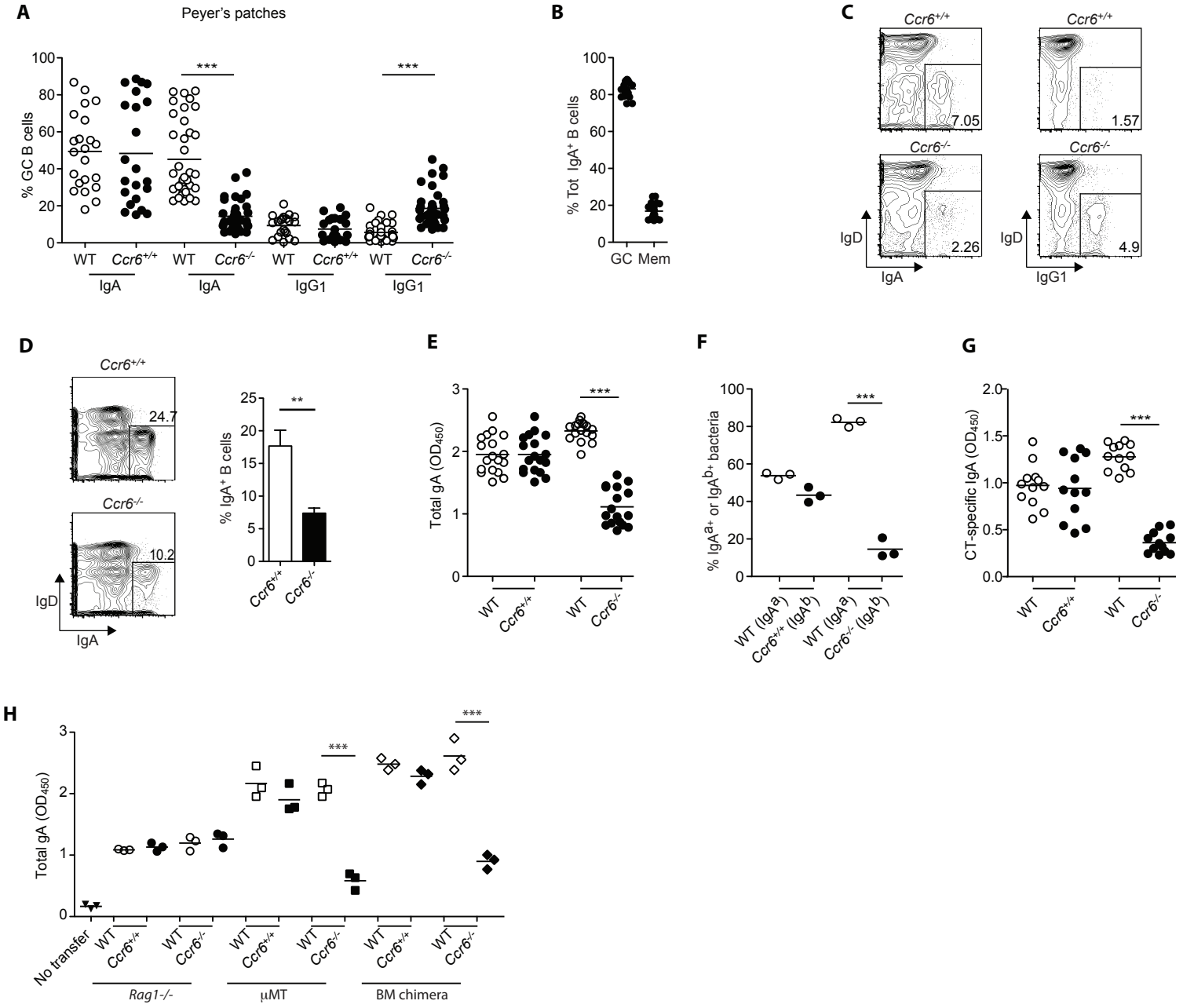

Reboldi at al.
Figure 2

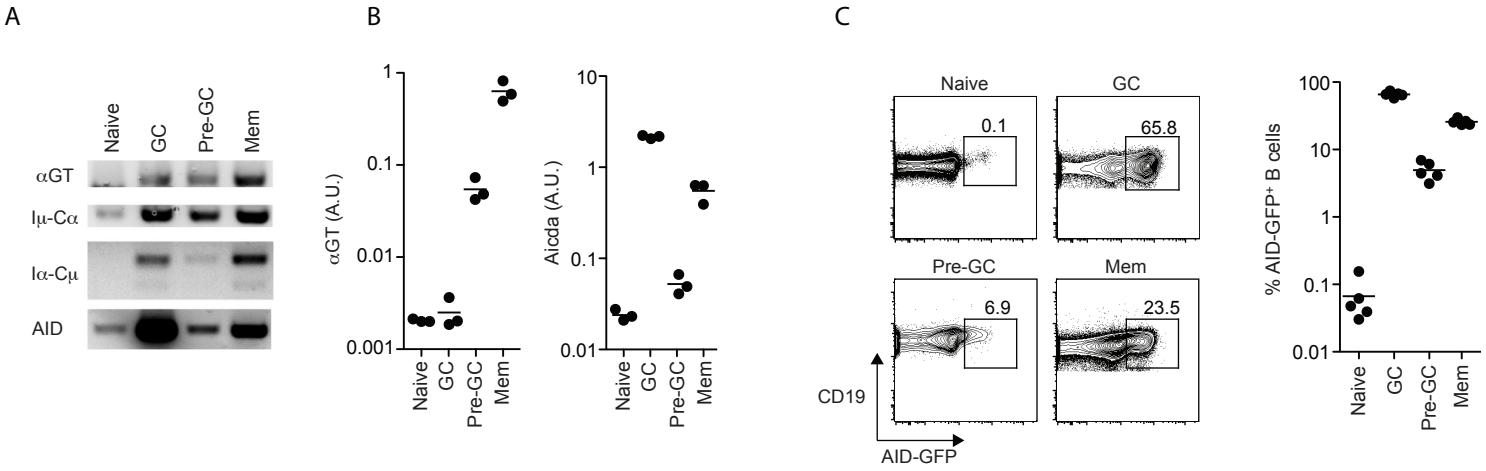

Reboldi at al.
Figure 3

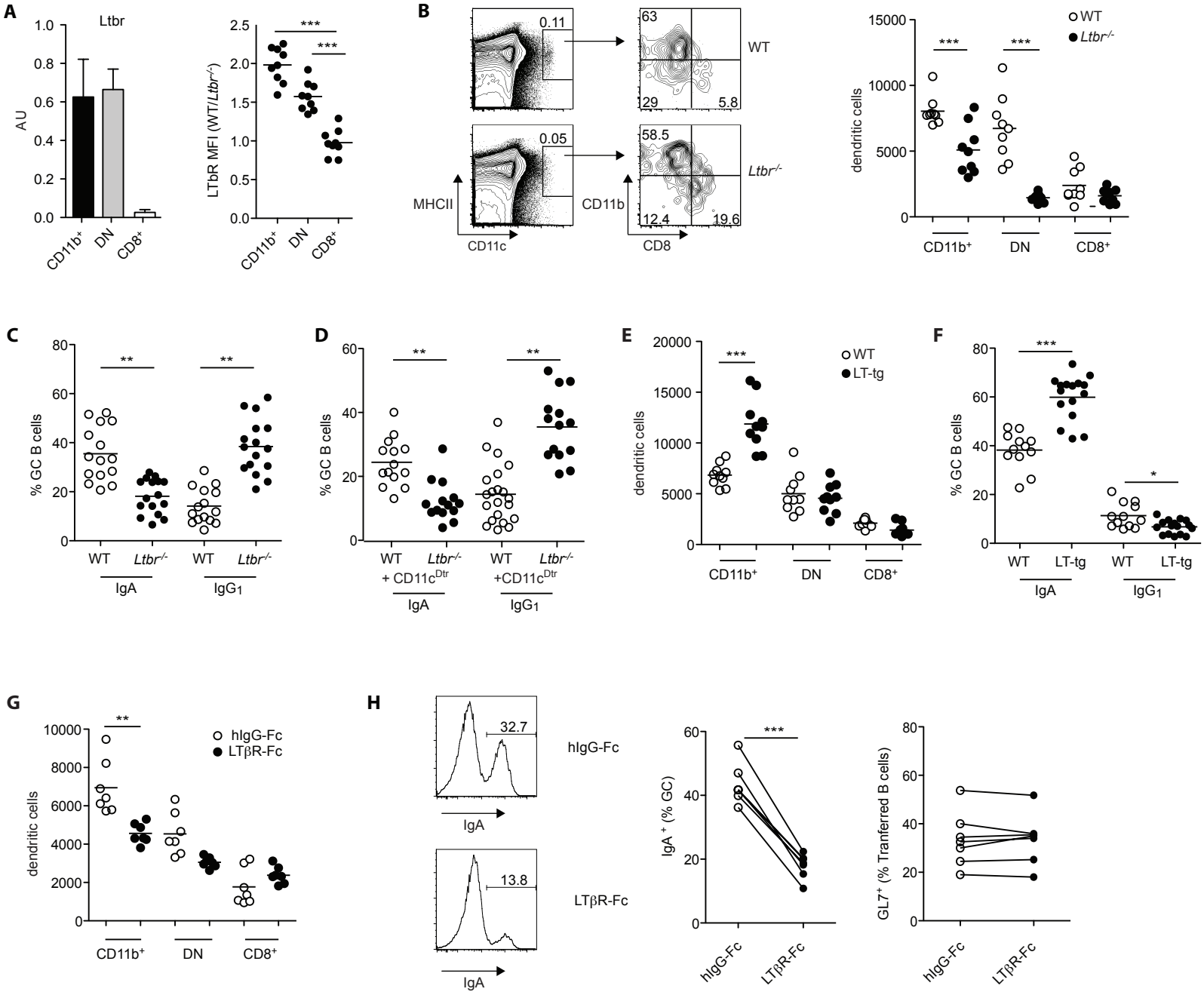

Reboldi at al.
Figure 4

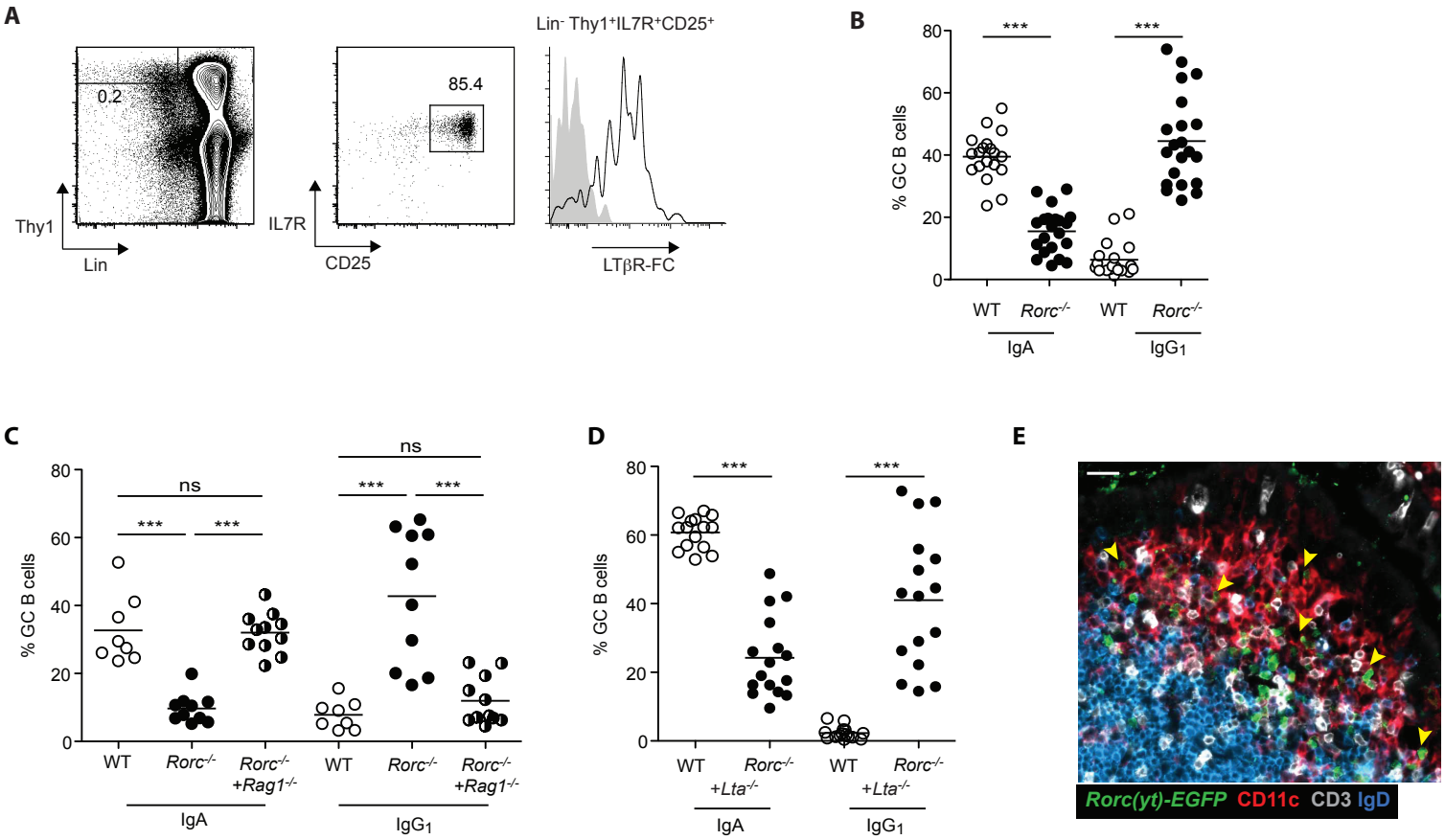

Reboldi at al.
Figure 5

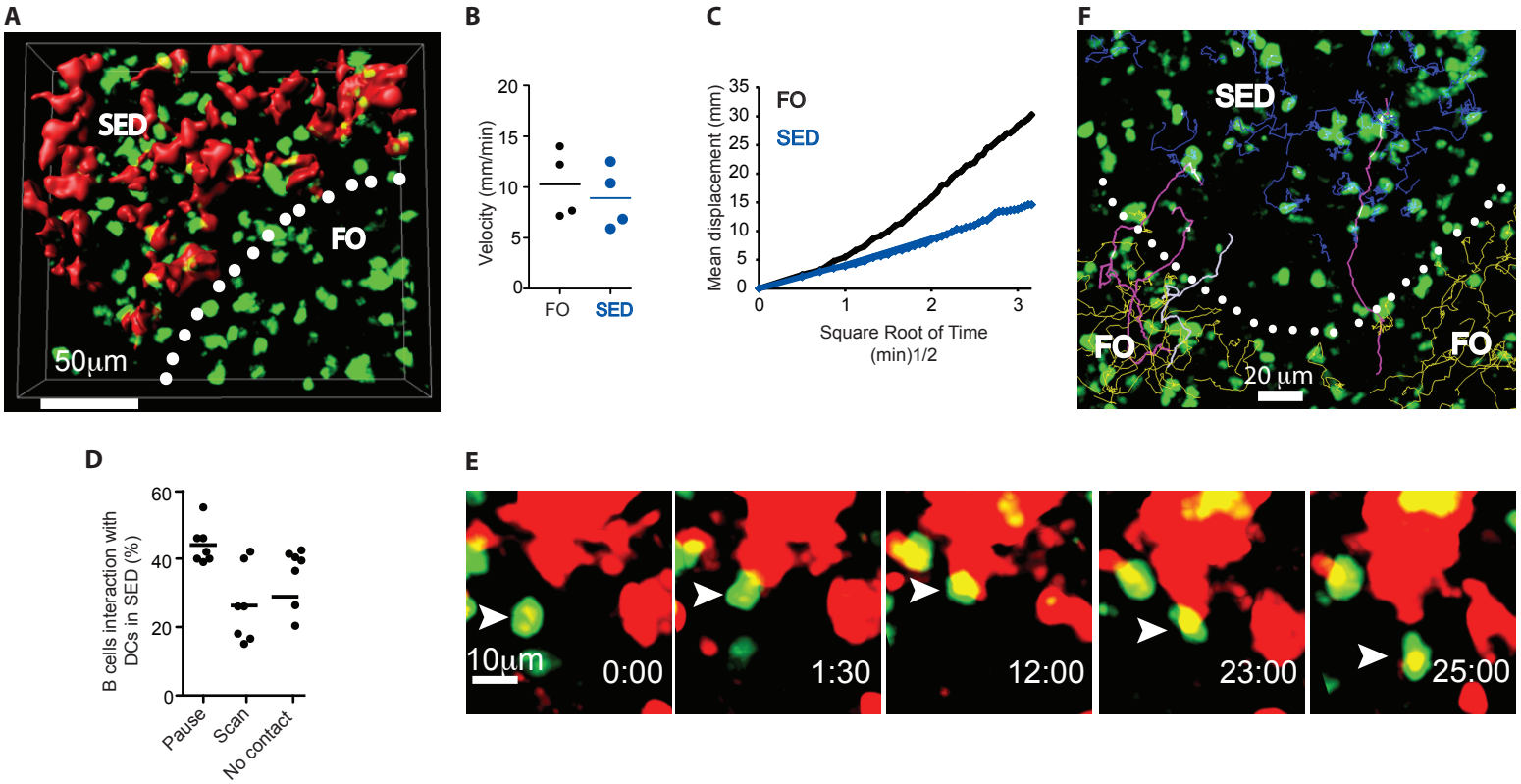

Reboldi et al.
Figure 6

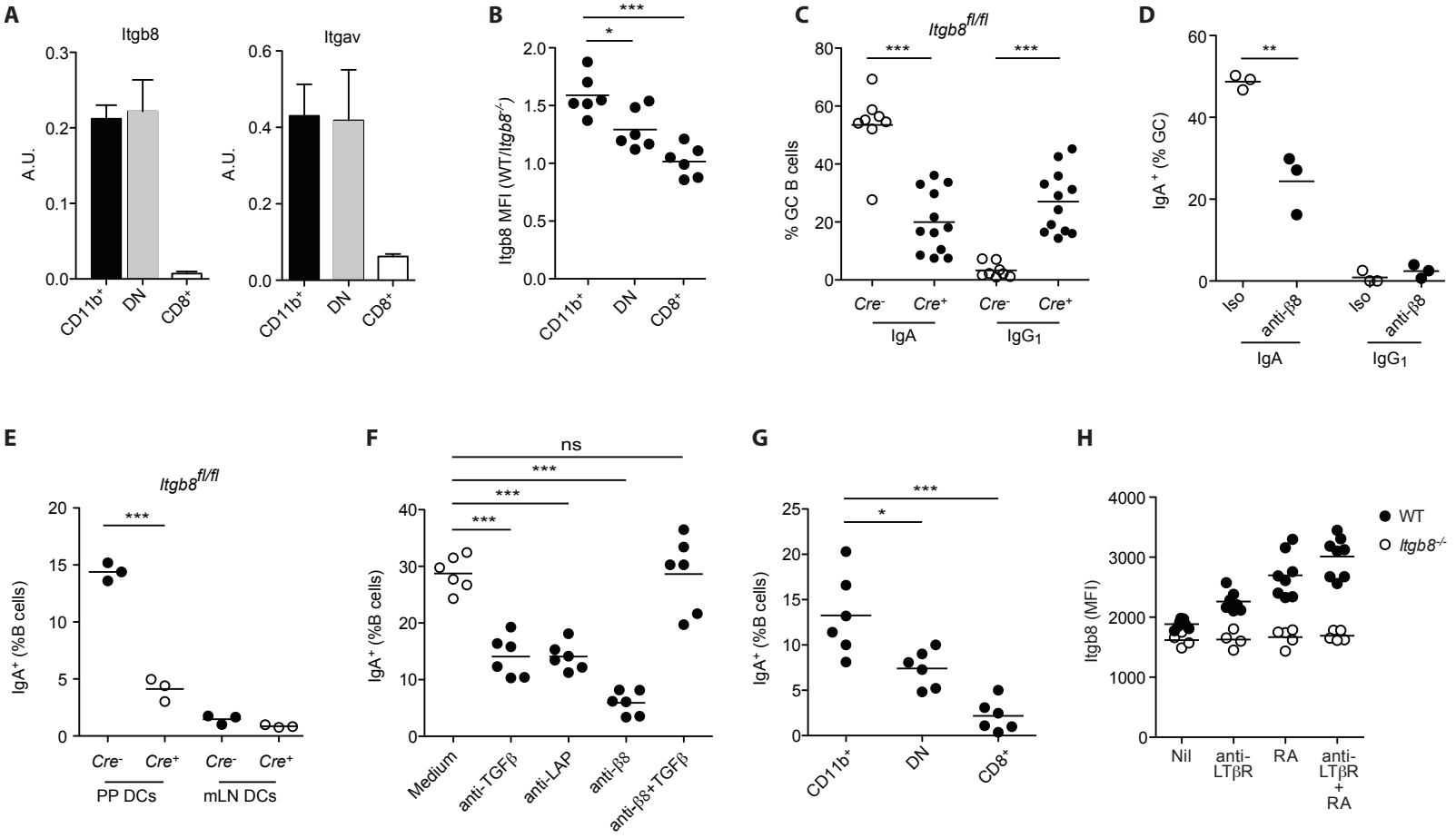
A
Itgb8
Itgav
A.U.
CD11b+
DN
CD8+
B
Itgb8 MFI (WT/Itgb8-/-)
C
Itgb8fl/fl
% GC B cells
Cre-
Cre+
IgA
IgG1
D
IgA+ (% GC)
Iso
anti-β8
E
IgA+ (%B cells)
PP DCs
mLN DCs
F
ns
Medium
anti-TGFβ
anti-LAP
anti-β8
anti-β8+TGFβ
G
H
Itgb8 (MFI)
WT
Itgb8-/-
Nil
anti-LTβR
RA
anti-LTβR + RA